Cellular Physiology and Biochemistry

Cell Physiol Biochem 2018;50:1068-1083
DOI: 10.1159/000494531
Published online: 24 October 2018
Accepted: 16 October 2018

Original Paper

Inhibition of Src Homology 2 Domain-Containing Protein Tyrosine Phosphatase-2 Facilitates CD31^{hi}Endomucin^{hi} Blood Vessel and Bone Formation in Ovariectomized Mice

Hao Yin[a,d] Jie Huang[a,d] Xu Cao[f] Zhen-Xing Wang[a] Jia Cao[a] Yin Hu[a,d]
Juan Luo[a] Yi-Juan Tan[a] Tuan-Hui Chen[a] Chun-Yuan Chen[a,d] Hui Xie[a,b,c,d,e]

[a]Movement System Injury and Repair Research Center, Xiangya Hospital, Central South University, Changsha, [b]Hunan Key Laboratory of Organ Injury, Aging and Regenerative Medicine, Changsha, [c]Department of Sports Medicine, Xiangya Hospital, Central South University, Changsha, [d]Department of Orthopedics, Xiangya Hospital, Central South University, Changsha, [e]China Orthopedic Regenerative Medicine Group (CORMed), Changsha, China, [f]Department of Orthopaedic Surgery, Johns Hopkins University School of Medicine, Baltimore, USA

Key Words
Shp-2 • Osteoporosis • Preosteoclast • Osteoclast • PDGF-BB • Angiogenesis

Abstract
Background/Aims: Recently, we and others showed that the relative abundance of a specific vessel subtype, strongly positive for CD31 and Endomucin (CD31^{hi}Emcn^{hi}), is associated with bone formation and bone loss, and platelet-derived growth factor-BB (PDGF-BB) secreted by preosteoclasts induces the formation of the specific vessels and thereby stimulates osteogenesis. Inhibition of Src homology 2 domain-containing protein tyrosine phosphatase-2 (SHP-2) has been shown to block the fusion of preosteoclasts into mature osteoclasts. However, it is unclear whether inhibition of SHP-2 could promote preosteoclast-induced angiogenesis and then enhance bone formation. This study aimed to determine the effects of a specific SHP-2 inhibitor (NSC-87877) on CD31^{hi}Emcn^{hi} vessel and bone formation. ***Methods:*** 3-month-old C57BL/6 mice were subjected to either ovariectomy (OVX) or sham operation. OVX mice were intraperitoneally injected with NSC-87877 and the control (sham) mice were treated with an equal volume of diluents (PBS). Two months later, bone samples from mice were collected for μCT, histological, immunohistochemical and immunofluorescent analyses to assess bone mass, osteogenic and osteoclastic acitivities, as well as the densities of CD31^{hi}Emcn^{hi} vessels. A series of angiogenesis- related assays were performed to test the effects of NSC-87877 on

H. Yin and J. Huang contributed equally to this work.

Hui Xie
and Chun-Yuan Chen
Movement System Injury and Repair Research Center, Xiangya Hospital, Central South University
#88 Xiangya Road, Changsha, Hunan 410008 (China)
E-Mail huixie@csu.edu.cn; chency19@csu.edu.cn

the pro-angiogenic activities of preosteoclasts *in vitro*. ***Results:*** We found that NSC-87877 is sufficient to induce bone-sparing effects in OVX-induced osteoporotic mouse model. We also found that NSC-87877 induces higher numbers of preosteoclasts and CD31^{hi}Emcn^{hi} vessels and higher levels of PDGF-BB in bone marrow of osteoporotic mice. *In vitro* assays showed that NSC-87877 prevents preosteoclast fusion, increases PDGF-BB production, and augments the pro-angiogenic abilities of preosteoclasts. ***Conclusion:*** Our results suggest that NSC-87877 can be used as a promising therapeutic agent for osteoporosis by inhibiting osteoclast formation and promoting preosteoclast-induced angiogenesis.

Introduction

Osteoporosis, characterized by low bone mass and microarchitectural deterioration of bone, is a systemic skeletal disease frequently seen in elderly people particularly in postmenopausal women [1]. Normal bone integrity is maintained by the coordinated balance between bone formation by osteoblasts and bone resorption by osteoclasts. However, estrogen deficiency after menopause often accelerates osteoclastic bone resorption and thereby leads to osteoporosis [2].

Postnatal bone homeostasis also depends on the formation of blood vessels, which mediate the transport of circulating cells, oxygen, nutrients, and a cornucopia of growth factors controlling bone growth and remodeling [3-5]. In 2014, researchers have identified a distinct blood vessel subtype called type H, which is characterized by high expression of CD31 and Endomucin (CD31^{hi}Emcn^{hi}) [6, 7]. These specific blood vessels were found to mediate the growth of the bone vasculature, maintain osteoprogenitors and couple angiogenesis to osteogenesis, but their numbers declined in aged animals and humans, which was accompanied by decreased osteoprogenitor counts and loss of bone mass [6-8]. Our previous study revealed that CD31^{hi}Emcn^{hi} blood vessels were also reduced in ovariectomized (OVX) mice (an experimental model of postmenopausal osteoporosis), whereas platelet-derived growth factor-BB (PDGF-BB) secreted by preosteoclasts was able to increase CD31^{hi}Emcn^{hi} vessel number and stimulate bone formation [9]. Thus, strategies designed to augment the formation of preosteoclasts and enhance CD31^{hi}Emcn^{hi} blood vessel generation may be beneficial for the prevention or treatment of bone loss, particularly for postmenopausal osteoporosis.

Src homology 2 domain-containing protein tyrosine phosphatase-2 (SHP-2), encoded by the *Ptpn11* gene, is a widely expressed protein tyrosine phoshatase (PTP) that plays important roles in the survival, proliferation, differentiation, and migration of various cell types [10]. A recent study by Zhou et al. revealed that inactivation of SHP-2 by using the osteoclasts-specific SHP-2 knockout mice or the SHP-2 inhibitor (NSC-87877) could markedly block the fusion of mononuclear preosteoclasts into multinucleated osteoclasts and impair the bone resorption activity of osteoclasts [11], suggesting that SHP-2 could potentially serve as a pharmacological target to inhibit osteoclastogenesis and increase the numbers of preosteoclasts. In consideration of the results of our previous study showing that preosteoclasts were capable of secreting PDGF-BB to stimulate CD31^{hi}Emcn^{hi} vessel formation and enhance osteogenesis, we hypothesized that inhibition of SHP-2 might be a promising approach for promoting the generation of this crucial blood vessel subtype, further enhancing bone formation and preventing estrogen deficiency-induced osteoporosis.

In the present study, we investigated whether the administration of a SHP-2 inhibitor (NSC-87877) could accelerate CD31^{hi}Emcn^{hi} blood vessel formation and increase bone mass in a mouse model of postmenopausal osteoporosis. We also studied *in vitro* the impacts of NSC-87877 on the production of PDGF-BB and the pro-angiogenic activities of preosteoclasts. The direct effects of NSC-87877 on endothelial angiogenesis as well as on osteogenesis and adipogenesis of mesenchymal stem cells (MSCs, the precursor cells of the osteoblast and adipocyte lineages) were also assessed. Our study aimed to determine the therapeutic

benefits of NSC-87877 in osteoporotic mice and to preliminarily elucidate the underlying mechanism.

Materials and Methods

Animals and treatments

Animal care and experimental procedures were approved by the Laboratory Animal Management Committee of Central South University. Thirty female C57BL/6 mice (3-months-old and weighing 25-30 g) were randomly and averagely divided into three groups. Mice were generally anesthetized and were subjected to bilateral ovariectomy (OVX; n=20) or a sham operation (Sham; n=10) as described previously [9, 12]. 2 weeks later, the OVX mice were intraperitoneally injected with NSC-87877 (2.5 mg/kg/day; OVX + NSC-87877 group; n = 10) or an equal volume of PBS vehicle (OVX group; n = 10). The sham-operated mice were also intraperitoneally injected with an equal volume of PBS every day. Two months later, bone marrow samples from tibias of mice were collected in heparin and centrifuged at 3000 rpm for 10 min. The supernatant was then obtained and stored at –80 °C until analyses. Uteri were isolated and weighed to confirm the success of OVX. Femora were also collected for further analyses.

Microcomputed tomography (μCT) analysis

Femora were dissected free from soft tissue, fixed in 4% paraformaldehyde for 48 h and analyzed by using Skyscan 1176 (Skyscan, Aartselaar, Belgium). The scanner was set at a current of 400 μA, a voltage of 50 kV, and a resolution of 8.88 μm per pixel. Images were reconstructed, analyzed and visualized by using the image reconstruction software (NRecon), data analysis software (CTAn v1.11) and three-dimensional model visualization software (μCTVol v2.2), respectively. Trabecular bone region of interest (ROI) was drawn starting from 0.15 mm proximal to distal epiphyseal growth plate and extended proximally for 0.4 mm length. The trabecular bone volume per tissue volume (Tb. BV/TV), trabecular thickness (Tb. Th), trabecular number (Tb. N) and trabecular separation (Tb. Sp) were measured.

Histological, immunohistochemical, and immunofluorescent analyses

For histological and immunohistochemical analyses, femora were dissected, fixed in 4% paraformaldehyde for 48 h, decalcified in 10% EDTA for 21 days, and embedded in paraffin. Samples were cut into 5-μm-thick longitudinally oriented sections of bone including the metaphysis and diaphysis. To assess the changes of trabecular bones, the osteogenic and osteoclastic activities in mice, hematoxylin and eosin (H&E) staining, immunohistochemistry staining for osteocalcin (OCN) and tartrate-resistant acid phosphatase (TRAP) were performed as described previously [9, 13].

Immunofluorescent analyses for CD31 and Emcn were performed to evaluate the extent of type H blood vessel formation and conducted as previously described [6, 7, 9]. Briefly, fresh femora were immediately fixed in ice-cold 4% paraformaldehyde for 4 h, decalcified in 18% EDTA for 3 days, dehydrated in 30% sucrose, and then embeded in OCT. Samples were cut into 30-μm-thick longitudinally oriented sections of bone including the metaphysis and diaphysis. Bone sections were then incubated with primary antibodies overnight at 4 °C, followed by incubation with the secondary antibodies at room temperature for 1 h. Sections incubated with secondary antibodies alone were used as the negative controls. Nuclei were stained with DAPI.

Images were acquired with an optical microscope (CX31; Olympus, Hamburg, Germany) or a fluorescence microscope (Leica DMI6000B, Solms, Germany). Positively stained cells, relative staining intensity or the number of $CD31^{hi}Emcn^{hi}$ vessel (HV) and total vessel (TV; positive for Emcn) were measured in at least three random visual fields per section. The numbers of adipocytes per square millimeter of bone marrow area (N/mm^2), preosteoclasts and osteoclasts per adjacent bone surface (N/mm) and the percentage of $CD31^{hi}Emcn^{hi}$ vessel (HV/TV; %) were calculated. TRAP staining kit was purchased from Sigma (St. Louis, MO, USA). The antibodies including anti-OCN, anti-CD31 and all secondary antibodies were obtained from Abcam (Cambridge, Cambs, Britain). Emcn antibody was purchased from Santa Cruz Biotechnology (Santa Cruz, CA, USA).

Cell culture

The macrophage cell line RAW264.7 was purchased from American Type Culture Collection (Rockville, MD, USA) and cultured in high glucose DMEM (Gibco BRL, Grand Island, USA) containing 10% fetal bovine serum (FBS; Gibco), 100 U/mL penicillin (Gibco) and 100 U/mL streptomycin (Gibco). Human microvascular endothelial cells (HMECs; Cell Bank of the Chinese Academy of Sciences, Shanghai, China) were cultured in MCDB131 medium (Gibco) containing 10% FBS (Gibco), 2 mM L-glutamine (Sigma), 1 μg/mL hydrocortisone (Sigma) and 10 ng/mL epidermal growth factor (EGF; Sigma). MSCs were prepared from male mouse strain C57BL/6- Tg(UBC-GFP)30Scha/J (Jackson Laboratory) and cultured in high glucose DMEM (Gibco) containing 10% FBS (Gibco), 100 U/mL penicillin (Gibco) and 100 U/mL streptomycin (Gibco). Cells were maintained at 37 °C in a humidified atmosphere containing 5% CO_2.

Preparation of conditioned media and TRAP staining

RAW264.7 cells (1.5×10^4/well) were seeded into 48-well plates and incubated with 100 ng/mL RANKL supplemented with 30 μM NSC-87877 or an equal volume of diluents (PBS). The negative control culture was grown in complete high glucose DMEM supplemented with an equal volume of vehicle. The culture medium was changed every 3 days. 6 days later, the conditioned media from un-induced (treated with an equal volume of PBS), RANKL-treated, or RANKL + NSC-87877-treated RAW264.7 cells were obtained and centrifuged at 2000 × g for 10 min to remove cellular debris. The supernatant was collected and stored at –80 °C or used for downstream experiments. The adherent cells were washed with PBS and fixed with 4% paraformaldehyde for 10 min. After washing with distilled water, cells were subjected to TRAP staining using a commercial kit (Sigma) according to the instructions provided by the manufacturer. $TRAP^+$ multinucleated cells showing more than three nuclei were identified as osteoclasts and counted under an inverted microscopy (Leica DMI6000B).

RNA interference

Three SHP-2 siRNAs (siSHP-2 #1, 2 and 3) and the universal negative control siRNA (Con siRNA) were obtained from RiboBio (Guangzhou, China). Cells transfection was performed according to the instructions of the manufacturers. In brief, RAW264.7 cells were transfected with siSHP-2 or Con siRNA using Lipofectamine 2000 (Invitrogen, Carlsbad, CA). 24 h later, the inhibitory efficiency of these siRNAs was verified by quantitative real-time PCR (qRT-PCR) analysis. The most effective siRNAs were used for investigating whether knocking down the expression of SHP-2 could affect the expression of PDGF-BB and VEGF in RANKL-treated macrophages. Briefly, RAW264.7 cells were incubated with 100 ng/mL RANKL and transfected with siSHP-2 or Con siRNA using Lipofectamine 2000. The negative control culture was grown in complete high glucose DMEM supplemented with an equal volume of Con siRNA. The culture medium was changed every 3 days. 6 days later, the cells and their conditioned media were obtained for testing the gene and secreted protein levels of PDGF-BB and VEGF, respectively. Target sequences for Con siRNA and siSHP-2 #1, 2 and 3 are as follows:

Con siRNA: 5'-TTCTCCGAACGTGTCACGT-3';
siSHP-2 #1: 5'-GAACCTTCATTGTGATTGA-3';
siSHP-2 #2: 5'-GTTAGGAACGTCAAAGAAA-3';
siSHP-2 #3: GAGATGTTATCGAGCTCAA-3'.

Enzyme-linked immunosorbent assay (ELISA)

The conditioned media and supernatant of bone marrow were collected and stored at –80 °C until they were thawed for the assay. The concentrations of PDGF-BB and VEGF were measured using commercial Mouse PDGF-BB ELISA Kit (Cusabio, Wuhan, China) and Mouse VEGF ELISA Kit (Multi Sciences LTD., Hangzhou, China) according to the manufacturer's instructions. The optical density of each well was determined with a microplate reader (Bio-Rad 680, Hercules, USA) set to 450 nm with wavelength correction set between 570 nm. The protein concentration of each sample was calculated from the standard curve.

Migration assay

For the scratch wound assay, HMECs (2×10^5 per well) were plated into a 12-well plate and incubated at 37 °C. After cells had attached, the monolayer was scratched using a pipette tip and washed with PBS to remove detached cells. Cells were then treated with conditioned media of RAW264.7 cells stimulated

by RANKL, RANKL + NSC-87877, or an equal volume of PBS. Cells were photographed at 0 h, 6 h and 12 h post-wounding. The rate of migration area was calculated as described previously [14]. Migration area (%) = $(A_0 - An)/A_0 \times 100$, where A_0 represents the area of initial wound area and An represents the remaining area of wound at the metering point.

For the transwell migration assay, HMECs (1×10^4 per well) were seeded into the upper chamber of a 24-well transwell plate (Corning, NY, USA) with 8-μm pore filters. The lower chamber was added with complete medium supplemented with conditioned media of RAW264.7 cells stimulated by RANKL, RANKL + NSC-87877, or PBS. After 12 h, cells on the upper surface of the filter membranes were removed by cotton swabs, while the migrated cells on the bottom side of the filter were stained with 0.5% crystal violet for several minutes. The number of migrated cells was counted under an optical microscope (Leica DMI6000B).

Cells proliferation assay

HMECs proliferation was examined by cell counting kit-8 assay (CCK-8; Dojindo, Kumamoto, Japan). Cells were seeded onto 96-well plates at a concentration of 5×10^3/well and treated with conditioned media from RAW264.7 cells stimulated by RANKL, RANKL + NSC-87877, or PBS. A group without cells served as the blank. At day 1, 2, 3, 4, and 5, CCK-8 solution (10 μL per well) was added to culture media and cells were incubated at 37 °C for 3 h. The absorbance was measured at 450 nm by a microplate reader (Bio-Rad 680) and the proliferation of cells was represented through the mean absorbance of each individual well minus the blank value.

Tube formation assay

HMECs were seeded onto Matrigel-coated 96-well plates at a concentration of 2×10^4 cells/well and treated with conditioned media from RAW264.7 cells stimulated by RANKL, RANKL + NSC-87877, or PBS. After 6 h, tube formation was detected by using an inverted microscope (Leica DMI6000B). Total branching points, total tube length and total loops per image were measured by a blinded independent observer.

qRT-PCR analysis

Total RNA was extracted using TRIzol Reagent (Invitrogen) and one μg of total RNA was reverse transcribed into cDNA with the RevertAid First Strand cDNA Synthesis kit (Fermentas, Burlington, Canada). Next, cDNA was amplified with FastStart Universal SYBR Premix ExTaq™ II (Takara Biotechnology, Japan) on an ABI PRISM® 7900HT System (Applied Biosystems, Foster City, USA). Relative gene expression was calculated using the $2^{-\Delta\Delta CT}$ method and GAPDH was used as a housekeeping gene for internal normalization. Primer sequences used for qRT-PCR were as follows: *m-Nfatc1*: forward, 5'-CAGTGTGACCGAAGATACCTGG-3', and reverse, 5'-TCGAGACTTGATAGGGACCCC-3'; *m-Atp6v0d2*: forward, 5'-AGCAA AGAAGACAGGGAG -3', and reverse, 5'-CAGCGTCAAACAAAGG-3'; *m-Mmp9*: forward, 5'-ACCCGAAGCGGACATT-3', and reverse, 5'-GGCATCTCCCTGAACG -3'; *m-Ctsk*: forward, 5'-GCGGCATTACCAACAT-3', and reverse, 5'-CTGGAAGCA CCAACGA-3'; *m-Ocstamp*: forward, 5'-GGGCTACTGGCATTGCTCTTAGT-3', and reverse, 5'-CCAGAACCTTATATGAGGCGTCA-3'; *m-Pdgf-bb*: forward, 5'-CCTCG GCCTGTGACTAGAAG-3', and reverse, 5'-CCTTGTCATGGGTGTGCTTA-3'; *m-Shp2*: forward, 5'-GGGGTCATGCGTGTTAGGAA-3', and reverse, 5'-ACTGCCA GACGGTTCTCTCT-3'; *m-Shp1*: forward, 5'-GGCCTCAGAGTCCCATTGGT-3', and reverse, 5'-GCTGAGGTCCCGGTGAAAC-3'; *m-Gapdh*: forward, 5'-CACCATG GAGAAGGCCGGGG-3', and reverse, 5'-GACGGACACATTGGGGGTAG-3'; *h-Vegf*: forward, 5'-ATCACCATGCAGATTATGCGG-3', and reverse, 5'-CCCCTTT CCCTTTCCTCGAAC-3'; *h-Gapdh*: forward, 5'-ATCC CATCACCATCTTCC-3', and reverse, 5'-GAGTCCTTCCACGATACCA-3'.

Osteogenesis and adipogenesis of MSCs

The effects of NSC-87877 on osteogenic and adipogenic differentiation potentials of MSCs were respectively evaluated using osteogenic and adipogenic differentiation media (Cyagen Biosciences, Guangzhou, China) as described previously [15, 16]. Briefly, MSCs were plated in 48-well plates and cultured in complete high glucose DMEM. After reaching 80% confluence, cells were washed with PBS and the medium was replaced with osteogenic or adipogenic medium supplemented with different concentrations of NSC-87877 or an equal volume of diluents (PBS). MSCs cultured in DMEM + 10% FBS were served as the negative control. Half of the medium was changed every 3 days. After 2 weeks (for Alizarin Red S staining) or 3 weeks (for Oil Red O staining), the cells were washed with PBS, fixed with 4% paraformaldehyde for

10 min, and then stained with the Alizarin Red S or Oil Red O solution (Solarbio, Beijing, China) according to the manufacturer's instructions. The stained cells were examined using an inverted microscope (Leica DMI6000B). The Alizarin Red S-positive area was analyzed by using Image-Pro Plus 6 software and shown as a percentage of Alizarin Red S-positive area over total area. Lipid droplets-containing cells were identified as adipocytes and counted in three fields of view per group.

Statistical analysis

Data are presented as means ± standard deviation (SD). The unpaired, two tailed Student's t-test was used to compare means between two groups. Analyses were performed using GraphPad Prism software and the differences were considered to be statistically significant when $P < 0.05$.

Results

NSC-87877 protects against OVX-induced osteoporosis

To test whether SHP-2 inhibition could induce protective effects on postmenopausal osteoporosis, OVX mice were established and intraperitoneally injected with NSC-87877 or an equal volume of diluents (PBS) once a day for eight weeks. Success of OVX was confirmed by markedly reduced uterus weight (Fig. 1A and B). μCT scanning was carried out to quantitatively and qualitatively evaluate bone mass and microarchitecture. As shown in Fig. 1C, OVX induced a prominent decrease of trabecular bone mass in the distal metaphysis

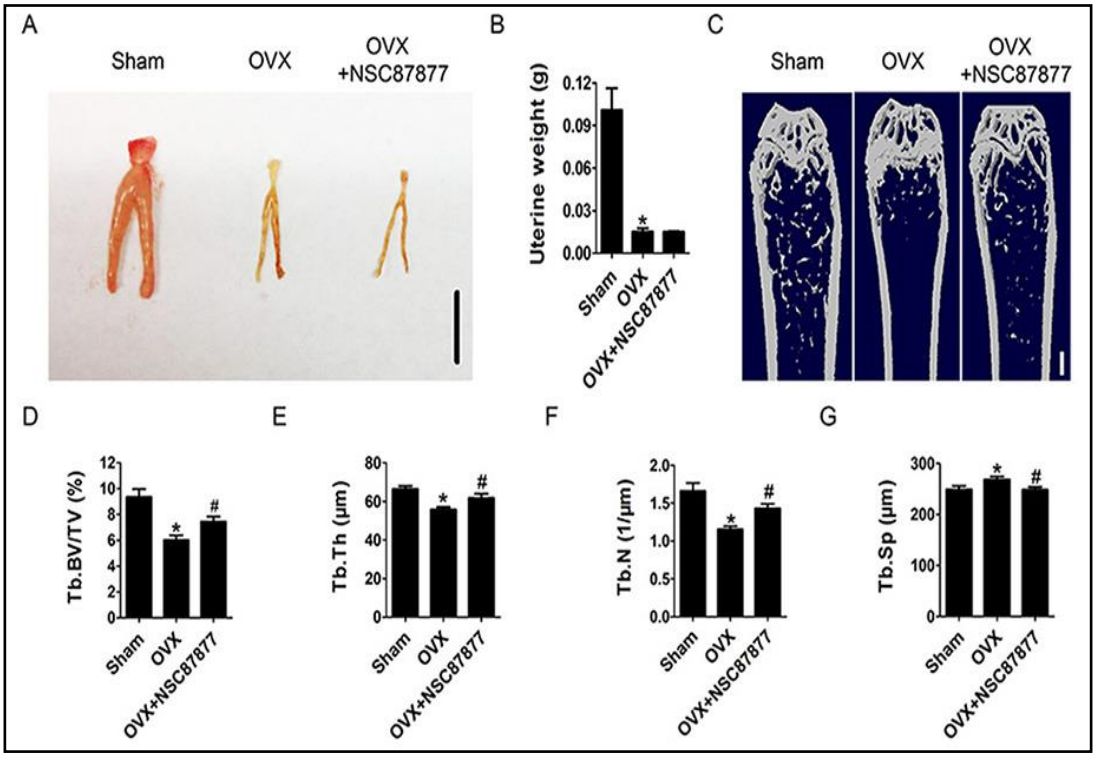

Fig. 1. NSC-87877 improves bone mass and microarchitecture in osteoporotic mice. (A) Representative images of uterus from mcice after sham-operation, ovariectomy (OVX) and OVX with NSC-87877 injection. Scale bar: 1 cm. (B) Quantitative analysis of uterus weight. n=5 per group. (C) Representative microcomputed tomography (μCT) images of distal femoral metaphysis from mice receiving different treatments. Scale bar: 1 mm. (D-G) Quantitative analyses of the trabecular bone fraction (Tb. BV/TV), trabecular thickness (Tb. Th), trabecular number (Tb. N) and trabecular separation (Tb. Sp) of femora from mice receiving different treatments. n=5 per group. *P<0.05 vs sham group, # P<0.05 vs OVX group.

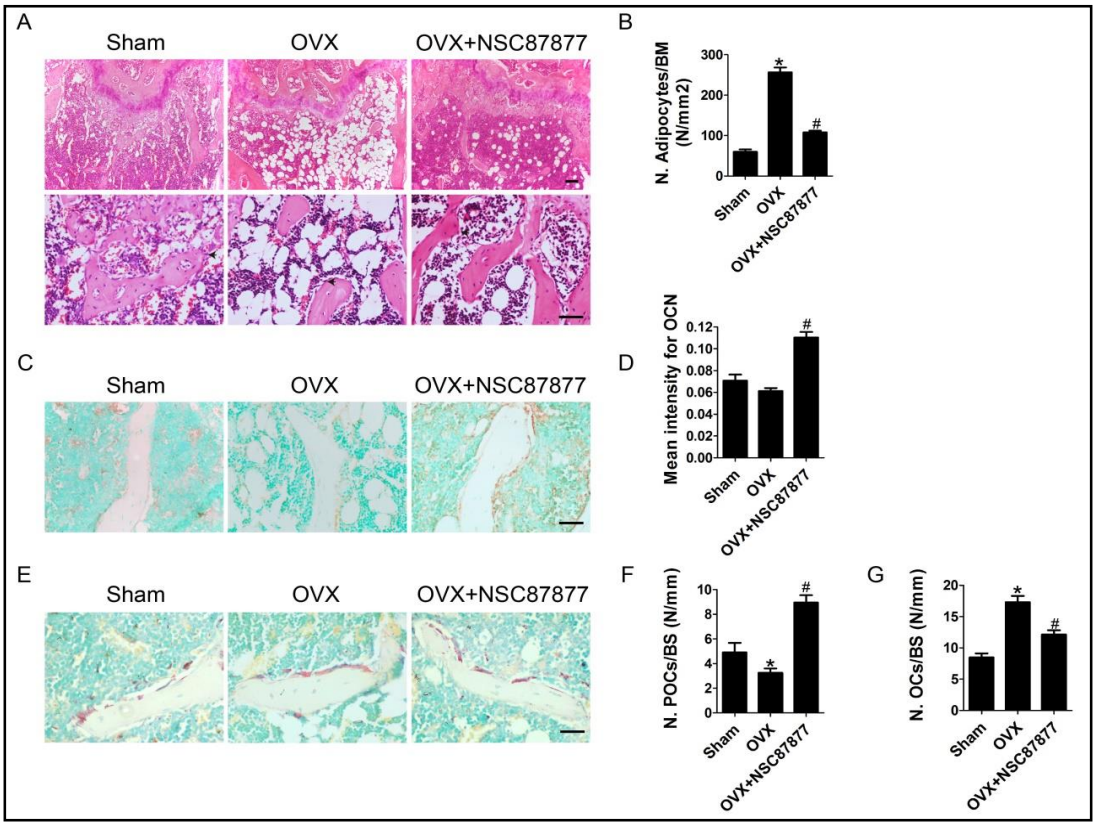

Fig. 2. NSC-87877 augments osteogenesis and reduces osteoclastogenesis in osteoporotic mice. (A) H&E staining of distal femoral metaphysis regions from mice after sham-operation, OVX and OVX with NSC-87877 injection. Scale bar: 100 μm (top) or 50 μm (bottom). (B) Quantitative analysis of the number of adipocytes in (A). n=3 per group. BM: bone marrow. (C) Representative images of immunohistochemical staining for OCN. Scale bar: 50 μm. (D) Quantitative analysis of the mean intensity for the OCN staining in (C). n=3 per group. (E) TRAP staining of femora from mice receiving different treatments. Scale bar: 50 μm. (F-G) Quantitative analyses of the numbers of TRAP$^+$ preosteoclasts and osteoclasts in (E). n=5 per group. POCs: preosteoclasts. OCs: osteoclasts. BS: bone surface. *P<0.05 vs sham group, $^{\#}$P<0.05 vs OVX group.

of the femur in mice, as compared with sham-operated mice. However, mice injected with NSC-87877 had significantly less bone loss. Quantitative measurements revealed that NSC-87877 markedly attenuated the OVX-induced reduction of trabecular bone volume fraction (Tb. BV/TV), thickness (Tb. Th), and number (Tb. N), as well as improved the trabecular separation (Tb. Sp) in the femur of mice (Fig. 1D-G), which further confirmed the preventive efficacy of NSC-87877 on postmenopausal osteoporosis.

In consistent with the above findings, histological analysis based on H&E staining also confirmed that trabecular bone changes in mice underwent OVX was obvious. In these mice, the trabecular bones became sparser and were surrounded with plenty of fat cells. On the contrary, OVX mice treated with NSC-87877 exhibited increased trabecular bones and decreased fat cells in bone marrow (Fig. 2A and B). OCN immunostaining showed that the osteogenic response of bone tissues was slightly reduced after OVX, whereas the administration of NSC-87877 markedly enhanced the osteogenic activity in OVX mice (Fig. 2C and D). As evidenced by TRAP staining, the number of osteoclasts on trabecular bone surface was profoundly increased in OVX mice compared to sham mice. However, a significantly higher number of TRAP$^+$ preosteoclasts and an apparently reduced number of osteoclasts were observed in NSC-87877-treated OVX mice (Fig. 2E-G), suggesting an inhibitory role of NSC-87877 in the fusion of preosteoclasts into osteoclasts. Our data indicate that SHP-2 inhibition can alleviate osteoporotic phenotypes induced by OVX.

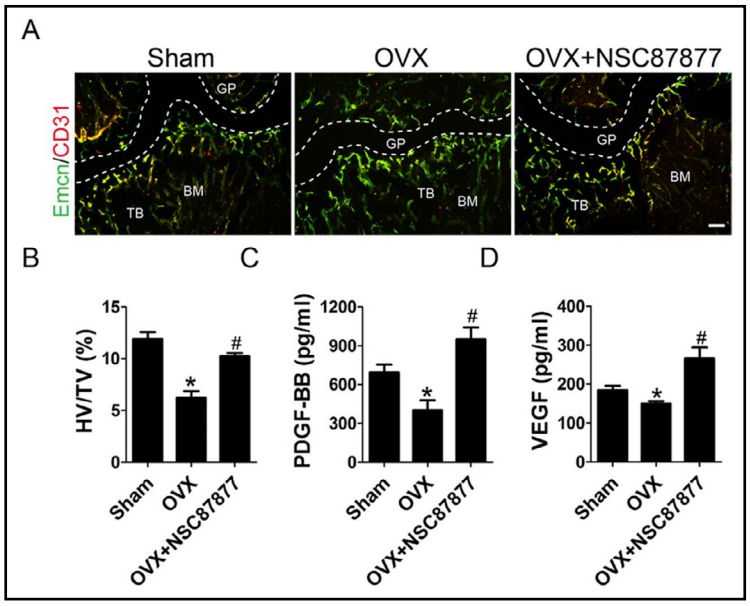

Fig. 3. NSC-87877 promotes CD31^{hi}Emcn^{hi} vessel formation and PDGF-BB production in bone marrow of osteoporotic mice. (A) Representative images of immunofluorescence staining for CD31 (red) and Emcn (green) in distal femoral metaphysis from mice after sham-operation, OVX and OVX with NSC-87877 injection. GP: growth plate. BM: bone marrow. TB: trabecular bone. Scale bar, 100 μm. (B) Quantitative analysis of the percentage of CD31^{hi}Emcn^{hi} vessel (HV; yellow) numbers in (A). n=3 per group. TV: total vessels. (C-D) The concentrations of PDGF-BB and VEGF in bone marrow from mice receiving different treatments were determined by ELISA. n=5 per group. *P<0.05 vs sham group, # P<0.05 vs OVX group.

NSC-87877 accelerates the formation of CD31^{hi}Emcn^{hi} blood vessels

We then asked whether inhibition of SHP-2 facilitated the formation of CD31^{hi}Emcn^{hi} blood vessels. As evidenced by immunofluorescence staining for CD31 and Emcn, the number of CD31^{hi}Emcn^{hi} blood vessels was significantly decreased in metaphysis of the femur in OVX mice compared to sham mice, consistent with our previous report[9]. Strikingly, the administration of NSC-87877 to OVX mice dramatically enhanced the percentage of this specific vessel subtype to a similar extent as in sham mice (Fig. 3A and B). ELISA analysis revealed that the concentrations of PDGF-BB and VEGF in bone marrow were significantly lower in OVX mice than that in control mice, whereas these pro-angiogenic proteins were markedly increased in OVX mice treated with NSC-87877 (Fig. 3C and D). Since PDGF-BB is the key effector that mediates the pro-angiogenic activities of preosteoclasts[9] and NSC-87877 is able to inhibit the fusion of preosteoclasts into osteoclasts [11], the promotion of preosteoclast PDGF-BB-induced angiogenesis may be a mechanism by which NSC-87877 prevents osteoporosis.

NSC-87877 blocks preosteoclasts fusion and facilitates PDGF-BB production in vitro

To confirm our hypothesis, we then verified the role of SHP-2 in the regulation of osteoclastogenesis and PDGF-BB production. RAW264.7 macrophages were cultured in medium containing RANKL and supplemented with NSC-87877 or an equal volume of PBS for 6 days. TRAP staining revealed that RANKL induced a significant increase in the numbers of TRAP$^+$ mononuclear preosteoclasts and multinucleated osteoclasts, but co-treatment with NSC-87877 prominently inhibited the ability of preosteoclasts to form mature osteoclasts (Fig. 4A and B). qRT-PCR analysis showed that the expression levels of genes responsible for osteoclast terminal differentiation, such as Nfatc1, Atp6v0d2, Mmp9, Ctsk and Ocstamp, were also markedly suppressed by NSC-87877 (Fig. 4C-G), which was consistent with the findings of a previous study[11]_ENREF_10. However, the mRNA level of Pdgf-bb was the most abundant in NSC-87877-treated cells (Fig. 4H). The conditioned media from cells treated with RANKL or RANKL + NSC-87877 were prepared for ELISA. Consistently, the data revealed that the concentration of secreted PDGF-BB was enhanced during RANKL-mediated osteoclast differentiation, and co-treatment with NSC-87877 resulted in greater production

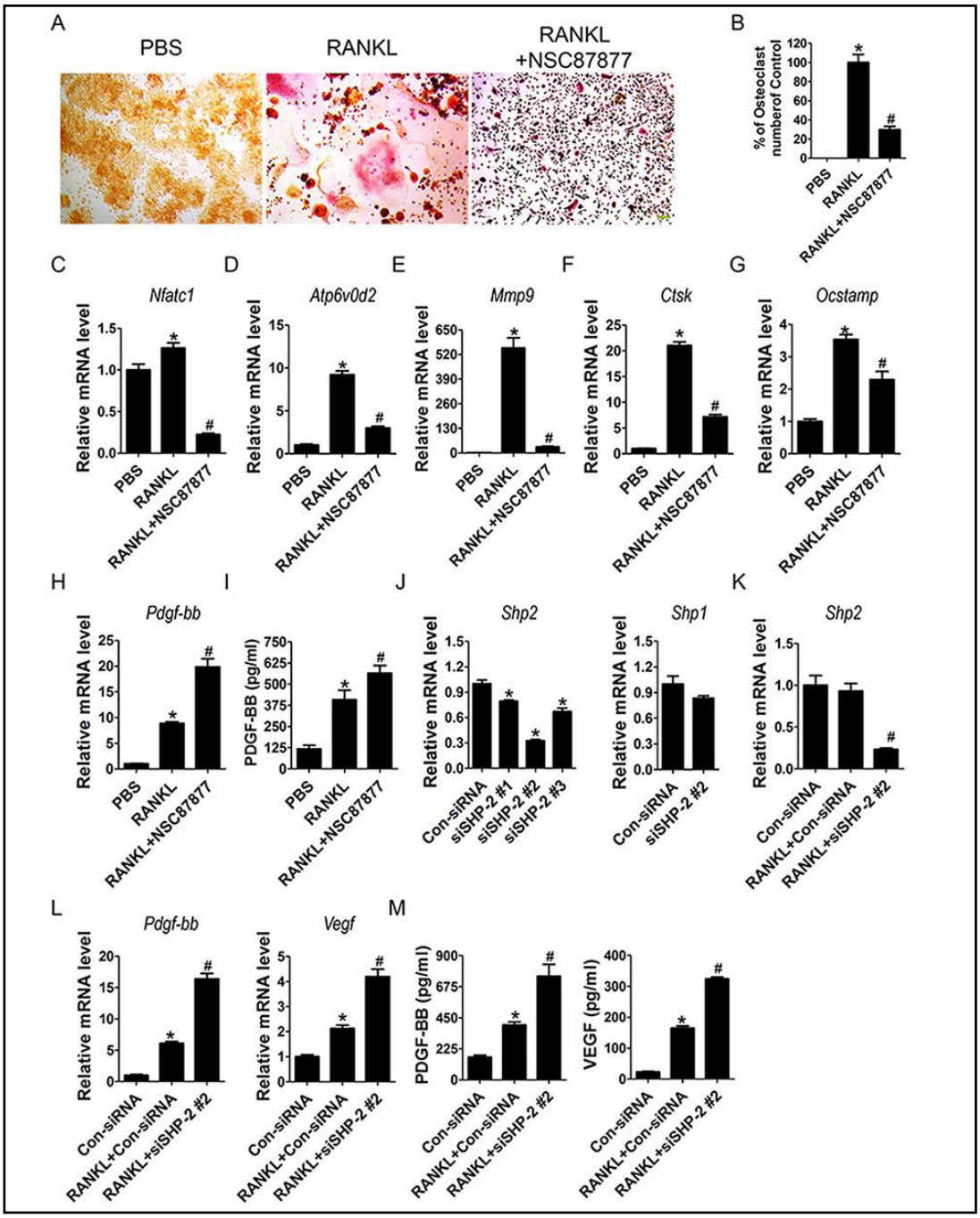

Fig. 4. NSC-87877 blocks preosteoclasts fusion and facilitates PDGF-BB production. (A) TRAP staining of RAW264.7 cells treated with PBS, RANKL and RANKL+NSC-87877. Scale bar: 50 μm. (B) Quantitative analysis of the percentage of osteoclast numbers relative to RANKL group. n=5 per group. (C-H) The expression levels of Nfatc1, Atp6v0d2, Mmp9, Ctsk, Ocstamp and Pdgf-bb were assessed by qRT-PCR analysis. n=3 per group. (I) The concentration of PDGF-BB in conditioned media from RAW264.7 cells receiving different treatments was determined by ELISA. n=5 per group. *P<0.05 vs control (PBS) group, # P<0.05 vs RANKL group. (J-K) The inhibitory efficiency of siRNAs targeting SHP-2 in non-treated and RANKL-treated RAW264.7 cells was verified by qRT-PCR analysis. n = 3 per group. (L) The expression levels of Pdgf-bb and Vegf were assessed by qRT-PCR analysis. n=3 per group. (M) The concentration of PDGF-BB and VEGF in conditioned media from RAW264.7 cells receiving different treatments was determined by ELISA. n=3 per group. * P<0.05 vs. Con siRNA group, # P<0.05 vs RANKL + Con siRNA group.

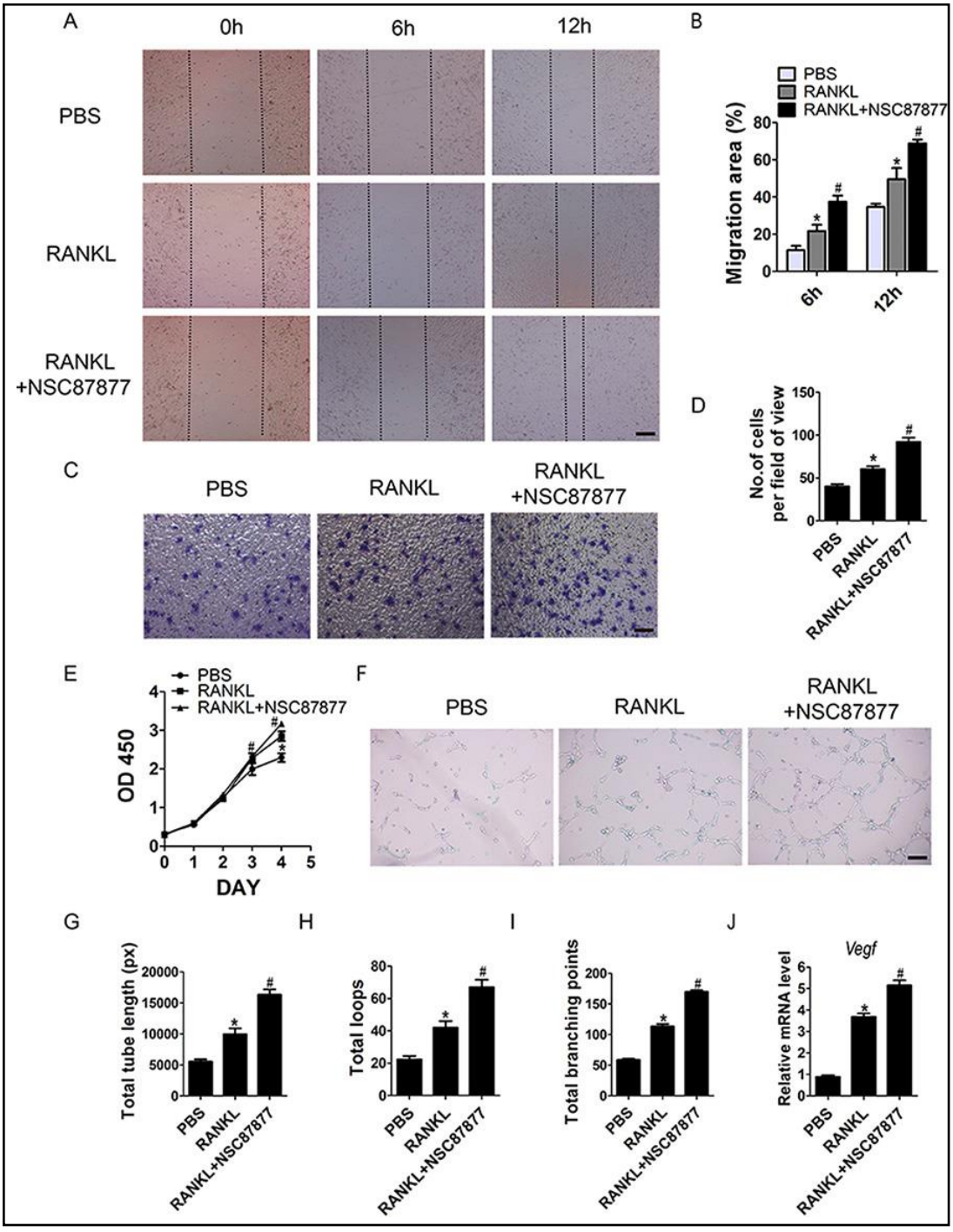

Fig. 5. NSC-87877 enhances the pro-angiogenic abilities of preosteoclasts. (A-D) The migration of HMECs stimulated by conditioned media from RAW264.7 cells treated with PBS, RANKL and RANKL + NSC-87877 was detected by the scratch wound assay (A-B) (Scale bar: 200 μm) and the transwell assay (C-D) (Scale bar: 100 μm). n=5 per group. (E) The proliferation of HMECs receiving different treatments was assessed by CCK-8 analysis. n=4 per group. (F) Representative images of tube formation assay on Matrigel in HMECs receiving different treatments. Scale bar: 200 μm. (G-I) Quantitative analyses of the total tube length, total loops and total branching points in (F). n=3 per group. (J) Detection of the expression of Vegf by qRT-PCR analysis. n=3 per group. *P<0.05 vs PBS group (cells treated with conditioned media from un-induced RAW264.7 cells), # P<0.05 vs RANKL group (cells treated with conditioned media from RANKL-treated RAW264.7 cells).

of PDGF-BB (Fig. 4I). Our results suggest that SHP-2 inhibition causes an accumulation of preosteoclasts and thereby enhances the level of pro-angiogenic factor PDGF-BB.

We also used three SHP-2 siRNAs (siSHP-2 #1, 2 and 3) to selectively knockdown SHP-2 expression in RAW264.7 macrophages and the inhibitory efficiency of these siRNAs was verified by qRT-PCR (Fig. 4J). siSHP-2 #2 showing the highest inhibitory efficiency was used for the following experiments. qRT-PCR analysis confirmed that SHP-1 expression was not altered by siSHP-2 #2 (Fig. 4J). We then explored whether siSHP-2 could affect the expression of PDGF-BB and VEGF in RANKL-stimulated RAW264.7 macrophages. The selectively inhibition of SHP-2 was determined by qRT-PCR (Fig. 4K). As shown in Fig. 4L and M, exposure of RANKL-stimulated macrophages to siSHP-2 resulted in significant increases in the mRNA level of Pdgf-bb as well as the levels of secreted PDGF-BB protein in the conditioned media, which was consistent with the effects of NSC-87877 on PDGF-BB expression. Specifically inhibition of SHP-2 by siSHP-2 also induced a profound up-regulation of the gene and protein levels of VEGF in RANKL-stimulated macrophages (Fig. 4L and M). The data further demonstrate the positive effects of SHP-2 inhibition on PDGF-BB and VEGF production by preosteoclasts.

NSC-87877 enhances the pro-angiogenic effects of preosteoclasts

To determine the impacts of SHP-2 inhibition on preosteoclast-induced angiogenesis, HMECs were incubated with the conditioned media from RAW264.7 macrophages stimulated by RANKL or RANKL + NSC-87877 for a series of angiogenesis-related assays. The scratch wound assay (Fig. 5A and B) and transwell assay (Fig. 5C and D) revealed that the conditioned media from RANKL-induced macrophages remarkably up-regulated the motility of HMECs

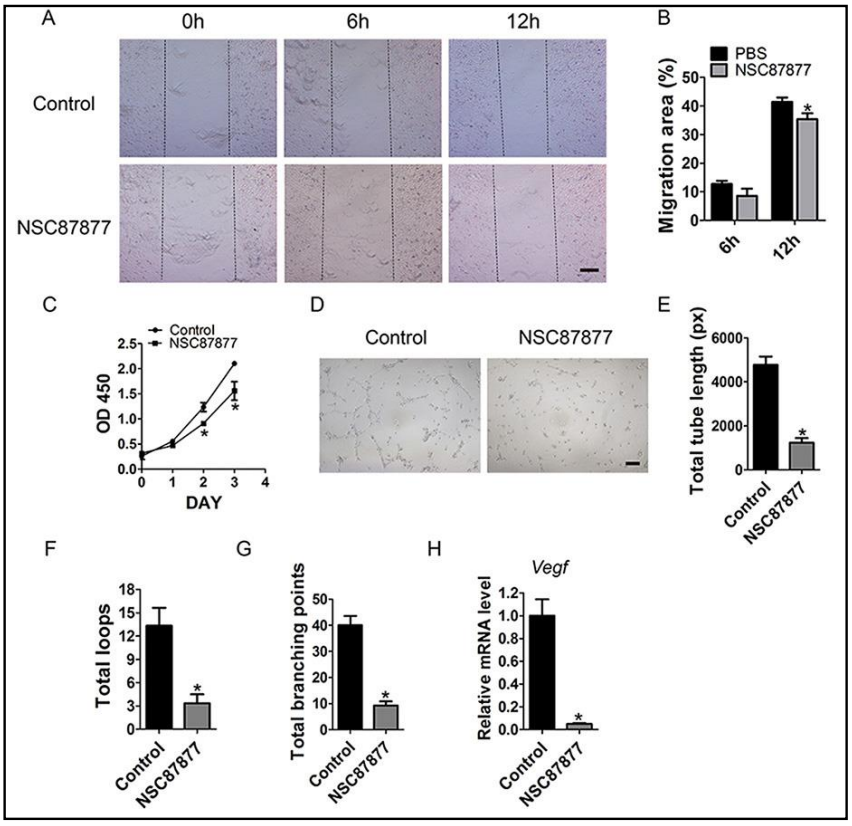

Fig. 6. Direct treatment of NSC-87877 down-regulates the angiogenic activities of endothelial cells. (A-B) The migration of HMECs stimulated by PBS or NSC-87877 was determined by the scratch wound assay. Scale bar: 200 μm. (C) The proliferation of HMECs receiving different treatments was assessed by CCK-8 analysis. n=4 per group. (D) Representative tube formation assay images in HMECs receiving different treatments. Scale bar: 200 μm. (E-G) Quantitative analyses of the total tube length, total loops and total branching points in (D). n=3 per group. (H) The expression of Vegf was detected by qRT-PCR analysis. n=3 per group. * P<0.05 vs control (PBS) group.

compared to conditioned media from un-induced macrophages, and HMECs migration was stimulated to the relatively greatest extent when exposure to conditioned media from RANKL + NSC-87877- treated cells. CCK-8 assay showed that HMECs proliferation was enhanced in response to conditioned media from RANKL-treated cells. Once the RANKL-induced macrophages were additionally treated with NSC-87877, the pro-proliferative effect of their conditioned media was much more obvious (Fig. 5E). The tube formation assay on Matrigel is an *in vitro* model of angiogenesis. The total tube length, total loops and total branching points were measured to quantify the ability of HMECs to form tubes. As shown in Fig. 5F-I, all the parameters were increased in HMECs stimulated with conditioned media from RANKL-treated cells, and conditioned media from RANKL + NSC-87877-treated cells exhibited much stronger pro-angiogenic activity on HMECs. The enhanced pro-angiogenic effect of conditioned media from RANKL + NSC-87877-treated cells was further confirmed by qRT-PCR assay for Vegf (Fig. 5J).

Considering the potential residual NSC-87877 in conditioned media might have a role in regulating HMECs function, we also assessed the direct effects of NSC-87877 on the angiogenic responses of HMECs. The results revealed that direct treatment with NSC-87877 induced significant reductions in the migration, proliferation, tube formation and Vegf expression of HMECs, as evidenced by scratch wound assay (Fig. 6A and B), CCK-8 assay (Fig. 6C), tube formation assay (Fig. 6D-G) and qRT-PCR analysis (Fig. 6H), respectively. Thus, the pro-angiogenic effects of conditioned media from RANKL + NSC-87877-treated RAW264.7 cells are not mediated by the residual NSC-87877. We also tested the direct effects of NSC-87877 on osteogenesis and adipogenesis of MSCs. As evidenced by Oil Red O staining, direct exposure to NSC-87877 induced a dose-dependent inhibition of adipogenic differentiation of MSCs (Fig. 7A and B). However, direct treatment with NSC-87877 did not interfere with the mineralized nodule formation of MSCs (Fig. 7C and D). Taken together, our *in vitro* functional assays suggest that SHP-2 inhibition augments the pro-angiogenic abilities of preosteoclasts and suppresses the adipogenic differentiation potential of MSCs, which may finally facilitate neovascular formation and bone regeneration.

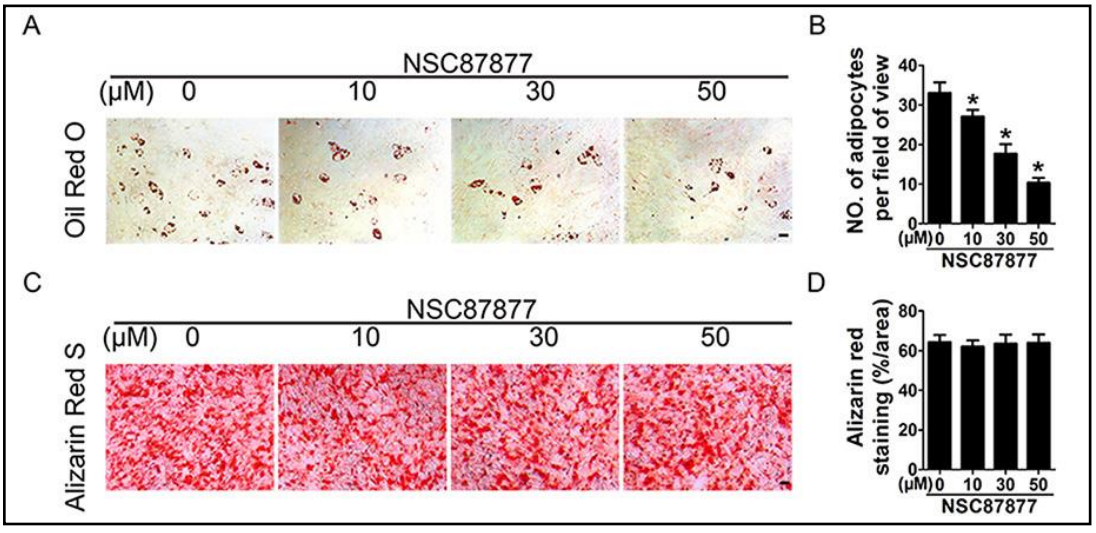

Fig. 7. Effects of NSC-87877 on osteogenesis and adipogenesis of mesenchymal stem cells (MSCs). (A) Oil Red O staining showed lipid droplet formation of MSCs receiving different treatments after adipogenic induction for 21 days. Scale bar: 50 μm. (B) Quantitative analysis of the numbers of lipid droplet-containing cells (adipocytes) in (A). n = 3 per group. (C) Alizarin Red S staining showed mineralized nodule formation of MSCs receiving different treatments after osteogenic induction for 14 days. Scale bar: 50 μm. (D) Quantitative analysis of the percentage of Alizarin Red S-positive area in (C). n = 3 per group. * P<0.05 vs control group (PBS group; 0 μM NSC-87877).

Discussion

Osteoporosis is one of the major public health issues and represents a considerable medical and socioeconomic burden for modern societies. Although numerous therapeutic attempts have been made to halt the progression of osteoporosis, the optimal prevention or treatment strategies are still being developed [17]. Here, we provided the first evidence that NSC-87877, a chemical inhibitor of SHP-2, could induce bone protective effects in ovariectomized osteoporotic mice, as defined by significantly elevated osteogenic activities and bone mass, as well as reduced osteoclast formation and bone destruction. Notably, we also found that NSC-87877 administration to OVX mice markedly enhanced the numbers of $CD31^{hi}Emcn^{hi}$ vessel subtype, and the concentrations of bone marrow PDGF-BB, a critical mediator of preosteoclast-induced angiogenesis. Using a series of assays *in vitro*, we determined that NSC-87877 treatment inhibited the fusion of preosteoclasts into osteoclasts, enhanced the level of secreted PDGF-BB, and augmented the pro-angiogenic abilities of preosteoclasts. Our results suggest that inhibition of SHP-2 induces the reduction of osteoclasts and the increase of preosteoclasts, thereby leading to attenuation of osteoclastic bone resorption, promotion of PDGF-BB-mediated angiogenesis and subsequent bone formation.

SHP-2 has been shown to be involved in the regulation of osteoclast development, skeletal remodeling, and bone mineral homeostasis. Germline mutations of SHP-2 in human result in skeletal abnormalities such as growth retardation and spinal curvature [18]. Global deletion of SHP-2 leads to early embryonic lethality [19, 20], and induced SHP-2-deficient mice exhibit an osteopetrotic phenotype and generate much fewer osteoclasts [21]. The role of SHP-2 in osteoclastogenesis has been confirmed by a recent report showing that SHP-2 is required for multinucleated osteoclast formation by promoting preosteoclast fusion via the RANKL/NFATc1 signaling axis [11]. Wang et al. generated monocyte/macrophage-specific SHP2 deficient mice and found that the mice exhibit mild osteopetrosis and their derived bone marrow macrophages have decreased osteoclast formation potential [22]. In consistent with these reports, our study determined that pharmacological inhibition of SHP-2 by NSC-87877 blocked the ability of preosteoclasts to form mature osteoclasts. Moreover, we used NSC-87877 to inhibit endogenous SHP-2 function and found that the osteoporotic phenotypes including in OVX mice were significantly alleviated. To the best of our knowledge, this study is the first to show the potential utility of NSC-87877 as a therapeutic reagent for postmenopausal osteoporosis.

NSC-87877 also affects SHP-1, another member of SH2-containing PTPs. However, previous studies have demonstrated that SHP-1 is a negative modulator of osteoclastogenesis, and mice lacking SHP-1 have increased number of osteoclasts [11, 23, 24]. Moreover, a recent study by Tang et al. showed that SHP-1 inhibition repressed osteoblast differentiation and mineralization [25]. In our study, the administration of NSC-87877 to OVX mice resulted in attenuated osteoclastic activity and elevated osteogenic responses, suggesting that the anti-osteoporotic effects by NSC-87877 cannot be attributed to SHP-1 inhibition.

Besides augmenting osteoblast activity and reducing osteoclast formation, it should to be noted that NSC-87877 treatment also resulted in a significant reduction in bone marrow fat cell deposition in OVX mice. Studies have revealed that excessive bone marrow adipocyte formation is tightly associated with development of osteoporosis and this occurs due to a shift in the differentiation of MSCs within bone marrow to favour the formation of adipocytes at the expense of forming osteoblasts [26-30]. Thus, inhibition of SHP-2 may reverse MSCs differentiation fate from adipogenesis to osteogenesis. However, although we found that direct exposure to NSC-87877 suppresses the adipogenesis of MSCs, osteogenic potential of MSCs is not promoted by NSC-87877.

It has been shown that induced SHP-2-deficient mice exhibit higher expression of bone formation markers [21], consistent with our present study showing that inhibition of SHP-2 by NSC-87877 enhanced the formation of osteoblasts in osteoporotic mice. However, a recent study reported that loss expression of SHP-2 specifically in MSCs resulted in an

absence of mature osteoblasts [31], indicating an essential role of SHP-2 in osteoblast formation. These paradoxical findings suggest that the pro-osteogenic effect of NSC-87877 is mediated through an indirect mechanism. Osteogenesis during bone modeling and remodeling is coupled with angiogenesis. Researchers identified a specific vessel subtype ($CD31^{hi}Emcn^{hi}$) in bone [6, 7] and the relative abundance of this vessel subtype is associated with bone formation and bone loss [6, 9]. Our previous study demonstrated that PDGF-BB secreted by preosteoclasts could promote formation of the specific vessels to induce the coupling of angiogenesis with bone formation [9]. Here, we found that the administration of a SHP-2 inhibitor (NSC-87877) enhanced the numbers of $CD31^{hi}Emcn^{hi}$ blood vessels in osteoporotic mice and the pro-angiogenic abilities of cultured preosteoclasts. NSC-87877 treatment also elevated PDGF-BB concentration in bone marrow of osteoporotic mice, as well as in the conditioned media of preosteoclasts. Thus, the promotion of preosteoclast-induced angiogenesis may be an important mechanism by which NSC-87877 stimulates osteogenesis and prevents osteoporosis. Taken together, all our findings suggest that inhibition of SHP-2 inhibits the adipogenic differentiation of MSCs and creates a beneficial microenvironment for osteogenesis and bone formation by promoting preosteoclast PDGF-BB-induced $CD31^{hi}Emcn^{hi}$ vessel generation. A limitation of our study is that although we have determined the effects of specific siRNAs targeting SHP-2 on PDGF-BB production by cultured preosteoclasts, we do not investigate the impacts of specific SHP-2 siRNAs on angiogenesis and bone formation *in vivo*.

Conclusion

In summary, our findings demonstrate that inhibition of SHP-2 by NSC-87877 stimulates $CD31^{hi}Emcn^{hi}$ vessel formation and increases bone mass in a mouse model of postmenopausal osteoporosis. The underlying mechanism may be the repression of osteoclast formation and the promotion of preosteoclast-induced angiogenesis, as NSC-87877 can block the fusion of preosteoclasts into mature osteoclasts, enhance the production of PDGF-BB and the pro-angiogenic abilities of preosteoclasts *in vitro*. Our study suggests that NSC-87877 can be used as a promising therapeutic agent for the prevention or treatment of postmenopausal osteoporosis.

Acknowledgements

This work was supported by the Excellent Young Scientist Award of National Natural Science Foundation of China (Grant No. 81522012), the National Natural Science Foundation of China (Grant No. 81670807, 81702237, 81600699), the Thousand Youth Talents Plan of China (Grant No. D1119003), the Hunan Youth Talent Project (Grant No. 2016RS3021), the Innovation Driven Project of Central South University (2016CX028), the Youth Foundation of Xiangya Hospital in Central South University (Grant No. 2016Q10), the Fundamental Research Funds for the Central Universities of Central South University (Grant No. 2018zzts895, 2017zzts032, 2017zzts014), Hunan Province Natural Science Foundation of China (Grant No. 2017JJ3501), and China Postdoctoral Science Foundation (Grant No. 2017M622614, 2017M612596).

Disclosure Statement

The authors declare no conflict of interests.

References

1 Rachner TD, Khosla S, Hofbauer LC: Osteoporosis: Now and the future. Lancet 2011;377:1276-1287.
2 Miyauchi Y, Sato Y, Kobayashi T, Yoshida S, Mori T, Kanagawa H, Katsuyama E, Fujie A, Hao W, Miyamoto K, Tando T, Morioka H, Matsumoto M, Chambon P, Johnson RS, Kato S, Toyama Y, Miyamoto T: HIF1α is required for osteoclast activation by estrogen deficiency in postmenopausal osteoporosis. Proc Natl Acad Sci U S A 2013;110:16568- 16573.
3 Huang B, Wang W, Li Q, Wang Z, Yan B, Zhang Z, Wang L, Huang M, Jia C, Lu J, Liu S, Chen H, Li M, Cai D, Jiang Y, Jin D, Bai X: Osteoblasts secrete cxcl9 to regulate angiogenesis in bone. Nat Commun 2016;7:13885.
4 Tomlinson RE, Silva MJ: Skeletal blood flow in bone repair and maintenance. Bone Res 2013;1:311-322.
5 Yang M, Li CJ, Sun X, Guo Q, Xiao Y, Su T, Tu ML, Peng H, Lu Q, Liu Q, He HB, Jiang TJ, Lei MX, Wan M, Cao X, Luo XH: Mir-497 approximately 195 cluster regulates angiogenesis during coupling with osteogenesis by maintaining endothelial notch and hif-1alpha activity. Nat Commun 2017;8:16003.
6 Kusumbe AP, Ramasamy SK, Adams RH: Coupling of angiogenesis and osteogenesis by a specific vessel subtype in bone. Nature 2014;507:323-328.
7 Ramasamy SK, Kusumbe AP, Wang L, Adams RH: Endothelial notch activity promotes angiogenesis and osteogenesis in bone. Nature 2014;507:376-380.
8 Wang L, Zhou F, Zhang P, Wang H, Qu Z, Jia P, Yao Z, Shen G, Li G, Zhao G, Li J, Mao Y, Xie Z, Xu W, Xu Y, Xu Y: Human type h vessels are a sensitive biomarker of bone mass. Cell Death Dis 2017;8:e2760.
9 Xie H, Cui Z, Wang L, Xia Z, Hu Y, Xian L, Li C, Xie L, Crane J, Wan M, Zhen G, Bian Q, Yu B, Chang W, Qiu T et al.: PDGF-BB secreted by preosteoclasts induces angiogenesis during coupling with osteogenesis. Nat Med 2014;20:1270-1278.
10 Wang G, Jin C, Hou Y, Zhang L, Li S, Zhang L, Wu B, Li Q, Xu C, Tian Y, Zhang L: Overexpression of shp-2 attenuates apoptosis in neonatal rat cardiac myocytes through the erk pathway. Exp Mol Pathol 2012;93:50-55.
11 Zhou Y, Mohan A, Moore DC, Lin L, Zhou FL, Cao J, Wu Q, Qin YX, Reginato AM, Ehrlich MG, Yang W: Shp2 regulates osteoclastogenesis by promoting preosteoclast fusion. FASEB J 2015;29:1635-1645.
12 Xie H, Xie PL, Luo XH, Wu XP, Zhou HD, Tang SY, Liao EY: Omentin-1 exerts bone-sparing effect in ovariectomized mice. Osteoporos Int 2012;23:1425-1436.
13 Li CJ, Cheng P, Liang MK, Chen YS, Lu Q, Wang JY, Xia ZY, Zhou HD, Cao X, Xie H, Liao EY, Luo XH: Microrna-188 regulates age-related switch between osteoblast and adipocyte differentiation. J Clin Invest 2015;125:1509-1522.
14 Zhang J, Chen C, Hu B, Niu X, Liu X, Zhang G, Zhang C, Li Q, Wang Y: Exosomes derived from human endothelial progenitor cells accelerate cutaneous wound healing by promoting angiogenesis through erk1/2 signaling. Int J Biol Sci 2016;12:1472-1487.
15 Chen CY, Rao SS, Ren L, Hu XK, Tan YJ, Hu Y, Luo J, Liu YW, Yin H, Huang J, Cao J, Wang ZX, Liu ZZ, Liu HM, Tang SY, Xu R, Xie H: Exosomal DMBT1 from human urine-derived stem cells facilitates diabetic wound repair by promoting angiogenesis. Theranostics 2018;8:1607-1623.
16 Tao SC, Yuan T, Zhang YL, Yin WJ, Guo SC, Zhang CQ: Exosomes derived from mir-140-5p-overexpressing human synovial mesenchymal stem cells enhance cartilage tissue regeneration and prevent osteoarthritis of the knee in a rat model. Theranostics 2017;7:180-195.
17 Adami S, Idolazzi L, Fracassi E, Gatti D, Rossini M: Osteoporosis treatment: When to discontinue and when to re-start. Bone Res 2013;1:323-335.
18 Kamiya N, Kim HK, King PD: Regulation of bone and skeletal development by the shp-2 protein tyrosine phosphatase. Bone 2014;69:55-60.
19 Yang W, Klaman LD, Chen B, Araki T, Harada H, Thomas SM, George EL, Neel BG: An shp2/sfk/ras/erk signaling pathway controls trophoblast stem cell survival. Dev Cell 2006;10:317-327.
20 Saxton TM, Henkemeyer M, Gasca S, Shen R, Rossi DJ, Shalaby F, Feng GS, Pawson T: Abnormal mesoderm patterning in mouse embryos mutant for the sh2 tyrosine phosphatase shp-2. EMBO J 1997;16:2352-2364.
21 Bauler TJ, Kamiya N, Lapinski PE, Langewisch E, Mishina Y, Wilkinson JE, Feng GS, King PD: Development of severe skeletal defects in induced shp-2-deficient adult mice: A model of skeletal malformation in humans with shp-2 mutations. Dis Model Mech 2011;4: 228-239.
22 Wang L, Iorio C, Yan K, Yang H, Takeshita S, Kang S, Neel BG, Yang W: A erk/rsk-mediated negative feedback loop regulates m-csf-evoked pi3k/akt activation in macrophages. FASEB J 2018;32:875-887.

23 Umeda S, Beamer WG, Takagi K, Naito M, Hayashi S, Yonemitsu H, Yi T, Shultz LD: Deficiency of shp-1 protein-tyrosine phosphatase activity results in heightened osteoclast function and decreased bone density. Am J Pathol 1999;155:223-233.
24 Aoki K, Didomenico E, Sims NA, Mukhopadhyay K, Neff L, Houghton A, Amling M, Levy JB, Horne WC, Baron R: The tyrosine phosphatase shp-1 is a negative regulator of osteoclastogenesis and osteoclast resorbing activity: Increased resorption and osteopenia in me(v)/me(v) mutant mice. Bone 1999;25:261-267.
25 Tang XL, Wang CN, Zhu XY, Ni X: Protein tyrosine phosphatase shp-1 modulates osteoblast differentiation through direct association with and dephosphorylation of gsk3beta. Mol Cell Endocrinol 2017;439:203-212.
26 Lu Q, Liu H, Cao T: Efficient isolation of bone marrow adipocyte progenitors by silica microbeads incubation. Stem Cells Dev 2013;22:2520-2531.
27 Muruganandan S, Roman AA, Sinal CJ: Role of chemerin/cmklr1 signaling in adipogenesis and osteoblastogenesis of bone marrow stem cells. J Bone Miner Res 2010; 25:222-234.
28 Jing H, Liao L, An Y, Su X, Liu S, Shuai Y, Zhang X, Jin Y: Suppression of ezh2 prevents the shift of osteoporotic msc fate to adipocyte and enhances bone formation during osteoporosis. Mol Ther 2016;24:217-229.
29 Guo Q, Chen Y, Guo L, Jiang T, Lin Z: Mir-23a/b regulates the balance between osteoblast and adipocyte differentiation in bone marrow mesenchymal stem cells. Bone Res 2016;4:16022.
30 You L, Pan L, Chen L, Gu W, Chen J: Mir-27a is essential for the shift from osteogenic differentiation to adipogenic differentiation of mesenchymal stem cells in postmenopausal osteoporosis. Cell Physiol Biochem 2016;39:253-265.
31 Lapinski PE, Meyer MF, Feng GS, Kamiya N, King PD: Deletion of shp-2 in mesenchymal stem cells causes growth retardation, limb and chest deformity, and calvarial defects in mice. Dis Model Mech 2013;6:1448-1458.